Article

Not peer-reviewed version

Oxide Metamorphic Manganese Ores: An Experimental Results of Heat Treatment

Ruslan Zairovich Safarov *, Jumat Beysembekovich Kargin, Assemgul Kalybekovna Zhandildenova *, Yelaman Kanatovich Aibuldinov *, Nikolai Ivanovich Vatin *, Jiwon Seo, Crispin Henry William Barnes, Luis De Los Santos Valladares

Posted Date: 1 February 2024

doi: 10.20944/preprints202402.0052.v1

Keywords: hausmannite; bixbyite; braunite; manganese ore; sintering

Article

Oxide Metamorphic Manganese Ores: An Experimental Results of Heat Treatment

Ruslan Zairovich Safarov [1,*], Jumat Beysembekovich Kargin [2,5], Assemgul Kalybekovna Zhandildenova [1,*], Yelaman Kanatovich Aibuldinov [3,*], Nikolai Ivanovich Vatin [4], Jiwon Seo [5], Crispin H.W. Barnes [6] and Luis De Los Santos Valladares [6,7,8]

1 Department of Chemistry, Faculty of Natural Sciences, L.N. Gumilyov Eurasian National University, Astana, 010000, Kazakhstan; ruslanbox@yandex.ru (R.Z. Safarov), zh_as80@mail.ru (A.K. Zhandildenova)
2 Department of Technical Physics, Faculty of Physics and Technical Sciences, L.N. Gumilyov Eurasian National University, Astana, 010000, Kazakhstan; kjb_orken@mail.ru
3 Department of Chemistry and Chemical Technologies, Faculty of Natural and Agricultural Sciences, Kh. Dosmukhamedov Atyrau University, Atyrau, 060011, Kazakhstan; elaman_@mail.ru
4 Peter the Great St. Petersburg Polytechnic University, St Petersburg, 195251, Russia; vatin@mail.ru
5 College of Science and Technology, Yonsei University, 1 Yonseidae-gil, Wonju, Gangwon-do, 26493, Republic of Korea; jiwonseo@yonsei.ac.kr
6 Cavendish Laboratory, Department of Physics, University of Cambridge, J.J. Thomson Ave., Cambridge, CB3 0HE, United Kingdom; chwb101@cam.ac.uk (C.H.W. Barnes), ld301@cam.ac.uk (L. de Los Santos Valladares), kjb_orken@mail.ru (J.B. Kargin)
7 Programa de Pós-Graduação em Ciências de Materiais, Centro de Ciências Exatas e da Natureza, Universidade Federal de Pernambuco, 50670-901 Recife-PE, Brazil
8 Laboratorio de Cerámicos y Nanomateriales, Facultad de Ciencias Físicas, Universidad Nacional Mayor de San Marcos, Lima, Ap. Postal 14-0149, Perú
* Correspondence: ruslanbox@yandex.ru (R.Z. Safarov); zh_as80@mail.ru (A.K. Zhandildenova); elaman_@mail.ru (Ye.K. Aibuldinov)

Abstract: The objective of this work is the study the crystal structure and elemental content of braunite-hematite and braunite-psilomelane oxide manganese ores by means of X-ray diffractometry (XRD), Energy Dispersion X-ray (EDX) analysis, and X-Ray fluorescent (XRF) analysis. It was found that heat treatments at 600, 800, and 1000 °C promote the phase transitions of the manganese ores to the formation of thermostable phases hausmannite and bixbyite without change in the metallic composition. The homogeneity of the structure increases with increasing temperature, which is expressed in the decreasing of the Mn content in the EDX spectra after sintering above 800 °C as well as in a decrease of the phase number to only two phases: bixbyite and quartz. Remarkably, the hausmannite phase is obtained in the fraction of 61% after sintering the braunite-hematite ore sample at 1000 °C for 4 h. Since hausmannite is widely used to produce building materials, electrodes, catalysts, and other materials, these results are promising for developing technologies for obtaining new products based on phases of manganese minerals at high temperatures.

Keywords: hausmannite; bixbyite; braunite; manganese ore; sintering

1. Introduction

Manganese ores are widely used in ferrous metallurgy. Manganese is the 12th most abundant element on the planet, covering about 0.1% of the Earth's crust. However, despite this abundance on the planet's surface, manganese minerals are widely disseminated, currently making it difficult to find high-grade deposits [1]. The shortage of high-grade manganese ores is due to the constant demand for them. Therefore, the focus is shifting to the development of cost-effective technologies for utilization of medium and low-grade manganese ores [2,3]. The Central Kazakhstan region

 doi:10.20944/preprints202402.0052.v1

contains numerous medium-grade manganese deposits, with an average Mn content ranging from 15% to 40%. Manganese carbonate and oxide ores are the primary sources for extracting manganese [4]. Manganese is used for the deoxidation and desulfurization of steel, and as an alloying additive for producing special grades of steel [5–7].

In the manganese ores, manganese is in the form of various complex oxides and hydroxides, carbonates, silicates and, less often, sulfides [8]. The most common minerals of manganese are: oxides and hydroxides (pyrolusite $MnO_2 \cdot xH_2O$, braunite $3Mn_2O_3 \cdot MnSiO_3$, hausmannite Mn_3O_4, manganite MnO(OH), vernadite $MnO_2(Mn,Fe,Ca)(O,OH)_2 \cdot nH_2O$, psilomelane $mMnO \cdot MnO_2 \cdot nH_2O$, hollandite $MnBaMn_6O_{14}$, and bixbyite $(Mn,Fe)_2O_3$), carbonates (rhodochrosite $MnCO_3$, manganocalcite $(Ca,Mn)CO_3$, kutnahorite and others), silicates (rhodonite $(Mn^{2+},Fe^{2+},Mg,Ca)SiO_3$, manganese-containing garnets, olivines $(Mn, Fe)_2[SiO_4]$, and pyroxenes $MnMgSi_2O_6$), amphiboles ($AB_2C_5T_8O_{22}W_2$) and others [9]. The differences in the content of oxides in manganese ore result from different geological processes in each region. The phase transitions of the oxide components of various ores are always characteristic and differ from each other. High temperature exposicion significantly influences the phase mineralogical composition since phase transitions occur [10]. In this way, new oxide components of manganese ores can be obtained by sintering under various conditions and it depends on the region of occurrence of the deposit.

The scientific problem in this research is finding ways to obtain target mineral phases like bixbyite ($Mn_2^{3+}O_3$) and hausmannite ($Mn^{2+}Mn_2^{3+}O_4$) from MnO_2. Numerous publications describe how to synthesize different manganese oxide phases, such as hausmannite. The most common ways are co-precipitation, sol-gel synthesis, and hydrothermal synthesis. For instance, the authors in reference [11] show the synthesis of hausmannite (Mn_3O_4) plate like nano-grains, coin-like nano-sphere, and nanopetal structures using three different protocols: co-precipitation route, sol-gel synthesis, and co-precipitation assisted hydrothermal synthesis. The preparation protocols dominate nanostructured materials' structural, morphological, optical, electrochemical, and magnetic properties.

Some studies on techniques for high-temperature reduction of manganese ores and the gas reduction behavior have been also reported. In reference [12], the high-energy milling method has been reported to synthesize hausmannite nanoparticles from manganese ores of West Sumatera deposit (Indonesia). The synthesis was carried out at 700 °C and milling time of 8 h, the size of the nanoparticles produced was 90.50 nm. X-ray Fluorescence (XRF) results showed that the manganese content was 84.139%. The crystal structure of the hausmannite phase was tetragonal. Similarly, the authors in reference [13] have shown that Mn/Fe ratio in the ore samples increases significantly at high-temperature treatments. At 700 °C, during 90 min, the concentration reaches 51.89% Mn and 14.79% Fe, with the Mn/Fe ratio of 3.5; which is close to the ferromanganese grade specifications.

About the morphological changes and phase transition of manganese oxides as a function of temperature, the literature reports examples of thermal transition between MnO, Mn_3O_4, Mn_5O_8, and Mn_2O_3 [14]. The structural variations and alterations of the ratio of Mn and O among the various oxidation states of Mn strongly affect the properties of the material and the way to regulate its preparation technique.

About the reduction of manganese ores, an interesting work about the sintering process of medium-grade pyrolusite manganese ore from Karangnunggal mine (West Java, Indonesia) at 1200 °C in methane gas has been reported [15]. It has been found that pyrolusite (MnO_2) was reduced to hausmannite (Mn_3O_4), manganosite (MnO), and manganese carbide (Mn_7C_3).

The transformation of MnO_2 to the MnO-rich phase at 950 °C is described in reference [16], which also reports that increasing the reduction temperature, the oxygen-to-manganese ratio decreases. In these reactions oxygen incorporated into the structure of oxides acts as a reducing agent undergoing oxidation from O^{-2} to O^0 form when detaching from the Mn. The reduction of MnO_2 to MnO follows the sequence:

$$MnO_2 \rightarrow Mn_2O_3 \rightarrow Mn_3O_4 \rightarrow MnO \quad (1)$$

Sorensen et al. studied Wessels (South African Republic), Groote Eylandt (Australia), Companhia Vale do Rio Doce (CVRD, Brazil), and Gabonese manganese ores with different chemical

compositions and complex mineralogical structures [17]. The authors report that MnO_2 is reduced to Mn_2O_3 and Mn_3O_4 upon sintering in air. Moreover, by sintering the manganese ores in hydrogen, the higher manganese oxides reduce to MnO and also the iron oxides into metallic iron.

The article [18] also reported an investigation of the raw manganese ore $CaMn_6SiO_{12}$ and the sintered manganese Mn_3O_4 and MnO. Under a vacuum, both raw and sintered manganese ore were reduced to MnO above 1200 °C. Meanwhile, in the air, manganese ore was reduced to Mn_3O_4 rather than MnO at temperatures above 800 °C. The higher melting temperature of the sintered manganese ore was also defined, which was interpreted in terms of a higher content of MnO due to high-temperature treatment.

Authors [19] presented that manganese ore from the Clarion-Clipperton Fracture Zone (Cook Island, Peru Basin) changed the main Mn-containing phases from asbolane ($NiMn_2O_3(OH)_4 \cdot H_2O$), lithiphorite ($Al_{0.65}H_2Li_{0.33}MnO_4$), manganese oxide ($MnO_2$), vernadite ($Mn(OH)_4$), chalcophanite ($H_6Mn_3O_{10}Zn$), and birnessite ($MnO_2$) to magnetite ($(Mn,Fe)_3O_4$), bixbyite ($Mn_2O_3$), manganese oxide ($\zeta Mn_2O_3$) after calcination. Thus, after the calcination process, the number of phases decreased, resulting in the formation of more thermally stable phases.

Most of the manganese oxide mineral phases are actively used in industry. Ground natural and synthetic pyrolusite ($MnO_2 \cdot xH_2O$, 63,2% Mn) is used to produce galvanic cells, batteries [20], and catalysts [21]. Braunite ($3Mn_2O_3 \cdot MnSiO_3$, 69,5% Mn) is used in the metallurgical and chemical industries to produce manganese [22]. Of particular interest is the mineral hausmannite, which has a wide range of applications and, as a result, is a popular product on the market [23]. It is used to produce trimanganese tetraoxide, which is used in producing light brown, yellow-brown, brown, and dark brown bricks, ceramic products, paving slabs, etc. Synthetic hausmannite as a pigment can be used for staining in mass and surface staining [23,24]. Compared with pyrolusite, it significantly increases efficiency, reducing the harmfulness and labor intensity of the process [23]. The use of this product reduces the water absorption of painted bricks compared to red bricks, improving the surface structure. The surface becomes smoother and more uniform, without burnt bubbles.

In recent years, catalytic oxidation has been considered as one of the most promising ways to convert toxic volatile organic compounds into low-toxic compounds, up to CO_2 and H_2O. Manganese oxides exhibit strong redox properties and are characterized by a much lower price compared to catalysts based on platinum group metals. Thus, the authors [25] investigated the catalytic activity, hydrothermal stability and durability of various Mn-based porous oxides ($SmMn_2O_5$, $SmMnO_3$, Mn_3O_4, Mn_2O_3) in the complete oxidation of ethanol and toluene. The catalytic activity of the catalysts was shown to be strongly dependent on their morphology, with Mn_3O_4 synthesized by the reduction method exhibiting the best activity in the oxidation of carbon monoxide and toluene [26].

Thus, the sintering of manganese ores in different conditions allows us to obtain different manganese oxide phases. However, the analysis of scientific materials in the scientific databases shows that there is a lack of researches devoted to the production of oxide phases from manganese ores by thermomechanical processing methods. It should be noted that not only in relation to manganese ores of Central Kazakhstan, but also at the global level, the description of the processes of obtaining such phases from ore is rare. This fact emphasizes not only the relevance, but also the lack of research in the field of manganese ore processing to obtain high-tech oxide products. Particularly, the change in the chemistry and mineralogy upon heating of the braunite-hematite and braunite-psilomelane oxide manganese ores of Central Kazakhstan, has not been clarified.

This paper focuses on the phase composition of the complex oxide metamorphic manganese ores located in Central Kazakhstan before and after sintering in the temperature range 600-1000°C in the air atmosphere. In this paper, the correlation between the sintering temperature and the elemental and phase compositions of ores was investigated by energy dispersion X-ray fluorescent element analysis (EDX), X-ray phase diffractometric analysis (XRD), and X-ray fluorescence analysis (XRF).

The paper is the part of the research project devoted to find new ways of using manganese ores of Central Kazakhstan to obtain oxide manganese phases as a technological products: colorants and catalysts. The results of work on the project serve for creation scientific and technical base necessary for launching new production in the territory of the Republic of Kazakhstan. The project is of high

 doi:10.20944/preprints202402.0052.v1

social and economic significance, as its implementation will lay the foundations for the organization of a new production of a competitive products from local raw materials.

2. Materials and Methods

Two manganese ore samples were collected from the Bogach and the Zhaksy deposits (Kazakhstan). Table 1 shows reserves and conventional content of Mn in ores of Bogach and Zhaksy deposits.

Table 1. Reserves of manganese ores of Bogach and Zhaksy deposits [27].

Deposit	Geographic coordinates	Reserves, thousand tons	Mn content, %
Bogach (sample 1)	49°44'43.4"N 68°57'16.5"E	5000	39.0
Zhaksy (sample 2)	51°56'26.7"N 67°21'52.1"E	2300	14.4

The Bogach manganese ore deposit was discovered in 1983-1986 and is located in central Kazakhstan's Nura district of the Karaganda region. Oxidized ores have earthy and powdery-lumpy textures. Minerals of primary manganese ores are basic braunite ($Mn^{2+}(Mn^{3+})_6SiO_{12}$), hematite ($\alpha$-$Fe_2O_3$), ankerite (less often, $Ca(Fe,Mg,Mn)(CO_3)_2$), friedelite ($Mn^{2+}{}_8Si_6O_{15}(OH,Cl)_{10}$), jacobsite ($(Mn^{2+},Fe^{2+},Mg)(Fe^{3+},Mn^{3+})_2O_4$), and nonmetallic minerals such as manganoan calcite ($(Ca,Mn)CO_3$), manganese in quartz (SiO_2), chlorite ($(OH)_2\cdot(Mg,Fe)_3(OH)_6$) and manganese in gypsum ($CaSO_4\cdot 2H_2O$). Minerals of oxidized manganese ores are pyrolusite ($Mn^{4+}O_2$), psilomelane ($(Ba,H_2O)_2Mn_5O_{10}$), vernadite ($(Mn^{4+},Fe^{3+},Ca,Na)(O,OH)_2.nH_2O$) and less often hollandite ($(Mn^{4+},Mn^{3+},Ti,Fe^{3+})_8O_{16}$), goethite ($\alpha$-(Mn,Fe)OOH), and braunite ($Mn^{2+}(Mn^{3+})_6SiO_{12}$) [28]. Table 2 shows the average component composition of manganese ore from the Bogach deposit.

Table 2. The average content of elements in the Bogach manganese ore [28].

Element	Content, %
Mn	39.88
Fe	10.43
SiO_2	6.78
Al_2O_3	2.20
CaO	5.75
MgO	0.70
P	0.021
S	0.032

The deposit of manganese Zhaksy ore is located in the Zhaksy district of the Akmola region [25,26]. The ore formations of the deposit are represented as oxide minerals: braunite, psilomelane, pyrolusite, and hausmannite ($Mn^{2+}Mn^{3+}{}_2O_4$). Nonmetallic minerals are quartz, calcite, chalcedony (trigonal SiO_2), chlorite, and sericite ($KAl_2(AlSi_3O_{10})(OH)_2$). An admixture of pyrite (FeS_2) and chalcopyrite ($CuFeS_2$) is also recorded occasionally. A special feature of the manganese ores from the Zhaksy deposit is the low content of harmful impurities such as phosphorus, sulfur, and nonferrous metals.

The samples present the form of broken fragments of rock (lump form). The samples were crushed in ball milling equipment for eight hours into 1-5 mm granules. Figure 1 shows photos of grinded samples. It can be seen that the ore sample of the Bogach deposit has a darker shade close to black, which is an indication of a higher concentration of manganese.

 doi:10.20944/preprints202402.0052.v1

(**a**) (**b**)

Figure 1. Manganese ore samples: (**a**) the Bogach deposit; (**b**) the Zhaksy deposit.

The grinded samples were sifted through a sieve with a diameter of 0.075 mm, then sintered in a muffle furnace at 600 , 800 and 1000 ˚C for 4 h. The samples were sintered in cupels made of calcium 59.42%, iron 35.97%, manganese 2.48%, and trace arsenic, rubidium, and strontium impurities. The material has the property of absorbing lead, based on which the lead content may be reduced.

X-ray diffraction (XRD) analysis was performed on an automatic diffractometer DRON-3 (Saint-Petersburg, Russia) with Cu-K_α radiation, using a β-filter. The analysis was carried out at U=35 kV, I=20 mA, shooting θ-2θ, detector 2 deg/min. X-ray phase analysis on a semi-quantitative basis was carried out using diffractograms of powder samples using equal samples and artificial mixtures. The quantitative ratios of the crystal phases were also determined. The diffractograms were interpreted using the ICDD PDF2 powder diffractometric database (Powder Diffraction File) and diffractograms of pure minerals. The elemental analysis was performed by energy dispersive X-ray fluorescent spectroscopy (EDX) before and after sintering in each temperature range by taking at least four spectra from each sample to obtain an average value on an energy dispersive X-Ray fluorescence spectrometer EDX-8000 (Shimadzu, Japan). The operating conditions of the device were: tube – Rh; voltage (kV) – 30-50; amperage (mA) – 100-1000; filter – none; time (sec) – 60; atmosphere – air, limits of detection of elements from carbon to uranium – $1 \cdot 10^{-3}$ %. Since the sample loading cell is made of rhodium material, the background value of the rhodium (Rh) amount was not considered when interpreting the study results. The oxide composition of the samples was carried out by X-Ray fluorescent analysis (XRF) on an X-ray multichannel spectrometer SRM-25 (Nauchpribor, Orel, Russia) by the gravimetric method at a temperature of 21 ˚C, an ambient humidity of 62% and a pressure of 0.95 bar.

3. Results and Discussion

3.1. Crystallochemical Description of Obtained Phases

Manganese (III) oxide, which precedes the formation of hausmannite, is a brown-black crystal, insoluble in water, with three main modifications:

- α-Mn_2O_3, rhombic syngony, kurnakite mineral;
- β-Mn_2O_3, cubic syngony, bixbyite mineral (cell parameters a=0,941 nm, Z=16);
- γ-Mn_2O_3, tetragonal syngony (cell parameters a=0,57 nm, c=0.94 nm).

A hausmannite phase is obtained by heating in the temperature range of 950-1100 °C from manganese (III) oxide. In general, this process proceeds according to scheme 2 [31–34]:

$$6Mn_2O_3 \xrightarrow{950-1100\ ^\circ C} 4Mn_3O_4 + O_2 \quad (2)$$

Hausmannite or trimanganese tetraoxide with the general chemical formula of Mn_3O_4 can also be represented as a subclass of complex oxides $Mn^{2+}Mn_2^{3+}O_4$, consisting of two- and trivalent manganese placed in a tetragonal crystal [35,36]. The theoretical chemical content of hausmannite is MnO 31,00 %; and Mn_2O_3 69,00 % (Mn 72%). It also contains FeO, ZnO, BaO, MgO, CaO, and Mn^{3+}, possibly substituting Fe or Mn^{2+} with Zn [36]. Its crystallographic characteristics are: tetragonal syngony, $D^{19}{}_{4h}$ of $I4_1$ /amd; a_0 = 5,76; c_0 = 9,44A; $a_0:c_0$=1:1,639; Z=4 and symmetry class ditetragonal-bipyramidal – 4/mmm (L_44L_25PC) [37–40]. In the crystal structure, the main forms are pseudotetrahedral. The mineral has a slightly deformed spinel lattice. Therefore, the mineral is not

 doi:10.20944/preprints202402.0052.v1

cubic, like spinel, but tetragonal. The inclusion of iron into the structure of hausmannite causes an increase in a_0 and a decrease in c_0. All oxygen atoms in the hausmannite structure are equivalent [38,41,42].

3.2. Elemental and Oxide Content of Products

The elemental composition of the raw samples and sintering samples at 600, 800, and 1000°C for 4 h was obtained by energy-dispersive X-ray spectroscopy. Tables 3 and 4 present the study results of the elemental composition of the samples.

Table 3. Results of studying the effect of sintering temperature on the elemental composition of braunite-hematite manganese ore (sample 1). RT: Room temperature.

Spectrum	**Elemental content, %**									
					RT					
	Mn	**Ca**	**Ba**	**K**	**Sr**	**Fe**	**Pb**	Zn	Ni	Cu
1	83.35	7.49	3.53	2.66	2.10	0.28	0.31	0.17	0.03	0.03
2	83.18	7.61	3.52	2.66	2.18	0.27	0.32	0.17	0.02	0.03
3	83.38	7.51	3.55	2.63	2.08	0.27	0.31	0.16	0.02	0.03
4	83.44	7.40	3.55	2.54	2.20	0.28	0.32	0.17	0.03	0.03
Average	83.33	7.50	3.53	2.62	2.14	0.27	0.31	0.16	0.02	0.03
					600 °C					
1	82.90	7.84	3.60	2.61	2.15	0.32	0.32	0.16	0.03	0.03
2	82.67	7.94	3.56	2.70	2.14	0.32	0.32	0.17	0.03	0.03
3	82.87	7.85	3.62	2.63	2.14	0.32	0.31	0.16	0.02	0.03
4	82.67	7.95	3.48	2.70	2.16	0.32	0.32	0.16	0.03	0.03
Average	82.77	7.89	3.56	2.66	2.14	0.32	0.31	0.16	0.02	0.03
					800 °C					
1	82.91	7.93	3.50	2.41	2.23	0.32	0.32	0.17	0.02	0.02
2	83.18	7.81	3.53	2.33	2.23	0.33	0.33	0.17	0.03	0.03
3	83.06	7.82	3.60	2.37	2.22	0.33	0.33	0.17	0.03	0.03
4	83.46	7.80	3.23	2.37	2.24	0.30	0.34	0.17	0.02	0.03
Average	83.15	7.84	3.46	2.37	2.23	0.32	0.33	0.17	0.02	0.02
					1000 °C					
1	84.35	7.11	3.18	2.02	2.49	0.30	0.24	0.18	0.03	0.06
2	84.54	7.11	3.19	2.04	2.36	0.26	0.23	0.17	0.03	0.03
3	84.14	7.39	3.34	1.99	2.35	0.29	0.26	0.17	-	0.02
4	84.43	7.31	3.18	2.07	2.23	0.28	0.22	0.17	0.02	0.03
Average	84.36	7.23	3.22	2.03	2.35	0.28	0.23	0.17	0.02	0.03

Table 4. Results of studying the effect of sintering temperature on the elemental composition of braunite-psilomelane oxide manganese ore (sample 2). RT: Room temperature.

Spectrum	**Elemental content, %**										
						RT					
	Mn	**Si**	**Fe**	**Al**	**K**	**Ba**	**Ca**	**Sr**	Cu	Zn	Ni
1	58.65	22.34	11.56	3.35	1.69	0.95	0.91	0.29	0.08	0.04	0.02
2	58.89	22.40	11.87	2.69	1.69	0.96	0.91	0.34	0.09	0.05	0.02
3	89.90	-	-	4.90	1.97	1.18	1.06	0.57	0.14	0.08	0.04
4	76.25	-	15.04	4.15	1.72	1.05	0.97	0.46	0.12	0.07	0.04
Average	70.92	11.18	9.61	3.77	1.76	1.03	0.96	0.41	0.10	0.06	0.03
						600 °C					
1	58,63	22.59	11.86	2.64	1.75	0.96	0.95	0.34	0.08	0.05	0.03
2	76.15	-	15.55	4.49	1.85	-	1.01	0.54	0.13	0.07	0.05

 doi:10.20944/preprints202402.0052.v1

3	74.90	-	15.26	5.08	1.79	1.10	1.00	0.50	0.12	0.07	0.04
4	89.05	-	-	5.55	2.06	1.24	1.11	0.56	0.15	0.08	0.04
Average	74.68	5.64	10.66	4.44	1.86	0.82	1.01	0.48	0.12	0.06	0.04
					800 °C						
1	58.06	22.79	11.52	3.12	2.00	0.98	0.92	0.33	0.08	0.04	0.03
2	60.96	23.10	8.28	3.03	2.11	1.03	0.94	0,32	0.08	0.04	-
3	60.85	23.11	8.24	3.24	2.03	1.02	0.96	0.32	0.08	0.04	-
4	63.18	23.32	8.75	-	2.16	1.01	0.95	0.35	0.09	0.05	0.03
Average	60.76	23.08	9.19	2.34	2.07	1.01	0.94	0.33	0.08	0.04	0.01
					1000 °C						
1	69.74	16.33	9.48	-	1.62	1.06	0.95	0.49	0.11	0.07	0.03
2	66.99	17.70	8.31	2.46	1.80	1.08	1.01	0.40	0.08	0.05	-
3	68.46	18.04	9.10	-	1.67	1.04	0.98	0.42	0.09	0.06	-
4	68.82	17.62	9.11	-	1.70	1.05	0.97	0.44	0.10	0.05	0.03
Average	68.50	17.42	9.00	0.61	1.69	1.05	0.97	0.43	0.09	0.05	0.01

* Within the limits of the instrument's sensitivity lead and arsenic were also detected in a trace amount (less than 0.03%).

The results show that the sintering process changes the structures of the studied samples. Before sintering, the braunite-psilomelane oxide manganese ore sample (sample 2) was heterogeneous regarding its structural group composition, with the range of the manganese content of 58.65 - 89.90% with an average value of 70.92±13.07%. After sintering at 1000 °C, the range of manganese content decreased to 66.99-69.74% with an average value of 68.50±0.98%. The decreasing average value is related to the transfer of Mn into the residual phase left on the melting crucible. The structure of the residual phase was not studied in this research.

The elemental content in different spectra can vary as the EDX analysis gets the spectra from focusing on different sample locations. The minimal variation in elemental content can be observed in a single-phase matter. Thus, the more differences in the elemental content values, the more differences there are in the phase composition. From this point of view, the results of EDX and XRD analyses are correlating. Analysis of the elemental contents shows that the peaks' presence, location, and intensity remain practically unchanged. The peaks' unchanging indicates a relatively stable elemental composition. The modification concerns compounds of elements - oxides, complex oxides, carbonates, silicates, and their phase transitions. The homogeneity of the structure of the sample under study is determined by the mineral structures' degree of crystallinity/amorphousness due to the ongoing phase transition processes under conditions of temperature changes, passing from less stable to more stable thermostable structures.

Table 5 shows the oxide composition of the initial samples obtained by XRF. LOI is the loss of ignition compounds such as water, carbon dioxide, carbon, hydrogen, partially sulfur dioxide, and trace elements. Based on the data obtained from the elemental analysis of the initial composition of the samples, it was found that in terms of the manganese content, the braunite-hematite ore is superior to the braunite-psilomelane oxide ore sample and contains about 83.35% Mn (MnO 70.032%) and, the total content of impurity elements does not exceed 16.5%. The lowest manganese content is found in the braunite-psilomelane oxide ore, which is about 71.0%. The braunite-psilomelane oxide ore is presented in manganese and iron oxide forms (51.407% and 6.096%, respectively). The impurity components' content is more than 29.0% due to the influence of silicates, iron oxides, alumina, lime, and magnesia. As a result, the ore has a heterogeneous structure and a dark brown color.

Table 5. Results of studying the oxide composition of the initial samples 1 and 2 obtained by XRF.

Sample	**Content of the determined components, %**										
	SiO_2	**TiO_2**	**Al_2O_3**	**Fe_2O_3**	**CaO**	**MgO**	**MnO**	**P_2O_5**	**K_2O**	Na_2O	LOI
1 (braunite-hematite)	58.65	22.34	11.56	3.35	1.69	0.95	0.91	0.29	0.08	0.04	0.02

 doi:10.20944/preprints202402.0052.v1

2 (braunite-psilomelane oxide)	58.89	22.40	11.87	2.69	1.69	0.96	0.91	0.34	0.09	0.05	0.02

* LOI is the loss of ignition compounds.

3.3. Phase Content of Products

Figure 2 shows the X-ray diffractograms of the samples. All the given diffraction peaks belong only to the specified phases. The characteristic diffraction reflections are noted, which makes it possible to identify the phases present. The figure shows diffractograms of the original braunite-hematite (ore sample 1) and braunite-psilomelane oxide (ore sample 2) manganese ore samples. In the initial state, ore sample 1 includes phases of hollandite, cryptomelane, braunite, calcite, manganese oxide (III), and quartz. The most conspicuous components are hollandite and cryptomelane, which appear in pairs at diffraction angles of 12,74°, 18,15°, 28.98°, 29.71°, 33.26°, 37.77°, 42.00°, 49.68°. Also, the braunite phase is accompanied by bixbyite, which appears on the diffractogram in pairs at angles of 33.26° and 54.87°. There are also associated minerals - calcite (29.71°) and quartz (26.93°). Phase composition of ore sample 2 in its initial state is more uniform and includes phases of hollandite associated with pyrolusite (28.96°, 37.74°), bixbyite (33.30°, 38.48°, 54.95°), quartz – as associated mineral at angles of 21.01°, 26.90°, 36.81°, 39.74°, 40.52°, 50.14°, 54.95°.

Figure 2(a) shows the diffractograms of the ore sample 1 after sintering at temperatures of 600, 800, and 1000 °C for 4 hours in air atmosphere. Table 6 shows the results of a semi-quantitative phase analysis of the manganese ore sample 1 in the initial state and after sintering in a given temperature range. After sintering at 600 °C, the braunite-hematite ore includes phases of hollandite and cryptomelane that appeared in pairs at angles of 12.62°, 18.21°, 29.01°, 29.75°, 37.78°, bixbyite (manganese oxide III) (33.29°), and quartz (26.93°). A narrowing of the hollandite and cryptomelane peaks and a slightly more conspicuous bixbyite peak are characteristic. Herewith, the semi-quantitative phase analysis shows an almost threefold increase in the content of the bixbyite phase in comparison with the original sample. At the same time, the content of the hollandite and cryptomelane phases remains practically unchanged.

After sintering at 800 °C, the braunite-hematite ore includes only phases of hollandite and cryptomelane that appeared together at angles of 28.90°, 37.75°, and bixbyite at angles of 33.27°, 38.45°, 54.93° (Figure 5). Herewith, the intensity of the peaks of hollandite and cryptomelane significantly decreases, and a clear peak characterizes the bixbyite phase at an angle of 33.27°. That change in phase content is also seen in the semi-quantitative analysis. Thus, the bixbyite content increases to 31%. Also, the ratio of cryptomelane increases by about 10%, while the ratio of hollandite decreases by 14%. Phase transitions with the accumulation of a more stable oxide form of manganese, bixbyite, begin to appear more actively here. After sintering at 1000 °C, XRD detects a variety of phases such as hollandite, cryptomelane, bixbyite, quartz, hausmannite, amesite, calcium magnesium aluminum oxide, and hematite. At the same time, the diffractogram clearly shows the dominance of the hausmannite phase, which appears by multiple conspicuous peaks in a wide range of diffraction angles (18.16°, 29.23°, 31.42°, 32.72°, 36.47°, 38.41°, 44.71°, 49.88°, 50.79°). This predominance in the content of the hausmannite phase is confirmed with the results of semi-quantitative phase analysis. The semi-quantitative fraction of the hausmannite phase in the sample reaches 61.7%. The sample also contains a significant fractions of Mg- and Al-containing components - calcium magnesium aluminum oxide ($Ca_{0.965}Mg_2Al_{16}O_{27}$) and amesite ($(Mg_2Al)(AlSiO_5)(OH)_4$) 16,6% and 7,1% respectively. The fraction of hollandite and cryptomelane is insignificant and amounts to 6 and 2.1%, respectively.

 doi:10.20944/preprints202402.0052.v1

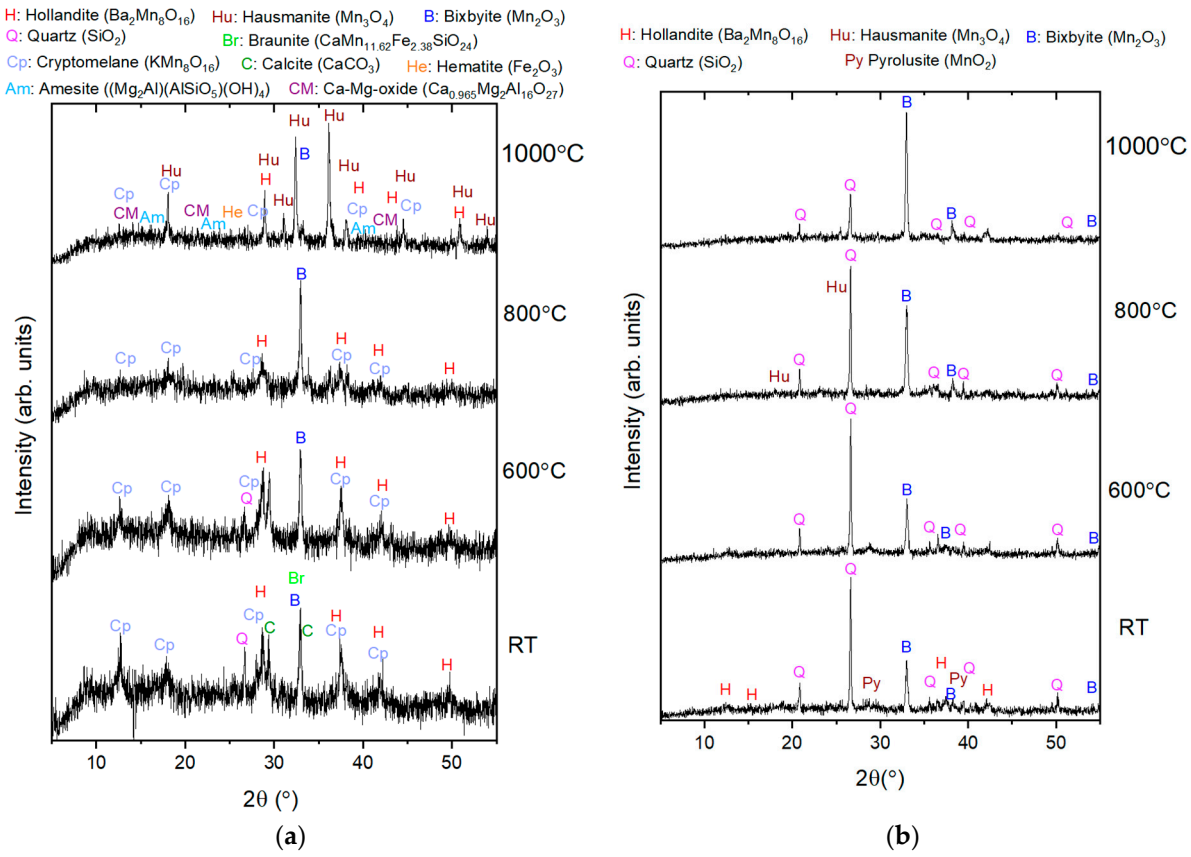

Figure 2. X ray diffractograms of the braunite-hematite (**a**) and braunite-psilomelane oxide (**b**) manganese ore samples after sintering at 600, 800, and 1000 °C during 4 h.

Figure 2(b) shows diffractograms of a manganese ore sample 2 after sintering at temperatures of 600, 800, and 1000 °C for 4 hours. Table 7 shows the results of a semi-quantitative phase analysis of sample 2 in the initial state and after sintering in a given temperature range. After sintering at 600 °C, the composition of braunite-psilomelane oxide ore includes bixbyite and quartz phases. Bixbyite is present in a smaller fraction - 30.7% and appears as a pronounced peak at a diffraction angle of 33.34°. Quartz in the composition of the sample is dominant and appears in pronounced peaks at angles of 21.02°, 26.91°, 36.85°, 39.73°, 40.58°, 42.68°, 50.11°, 55.07°. The quartz ratio in the sample reaches 69.3%. After sintering at 800 °C bixbyite peaks become more pronounced and appear at several diffraction angles - 33.30°, 35.93°, 38.51°, 54.96°. The quartz phase is still quite intense. Quartz is detected at angles of 21.01°, 26.88°, 39.73°, 45.87°, and 50.11°. At the same time, traces of hausmannite begin to appear in the sample's composition, with many insignificant marks on the diffractogram. The data obtained are consistent with the results of the semi-quantitative phase analysis. The sample contains phases of the following ratios: bixbyit - 38,9%, quartz - 54,6%, hausmannite – 6,5%. However, the hausmannite phase is no longer detected on the diffractogram of the ore sample 2 after sintering at 1000 °C. The diffractogram shows peaks of bixbyite (33.28°, 38.46°, 54.94°) and quartz (20.98°, 26.88°). However, in this case, bixbyite becomes the dominant phase. Bixbyite fraction reaches 69.1%, and quartz fraction remains 30.9%.

Table 6. Semi-quantitative phase ratios of braunite-hematite manganese ore sample.

Mineral	Chemical formula	Fraction, %			
		at RT	Sintering temperature, °C		
			600	800	1000

 doi:10.20944/preprints202402.0052.v1

Hollandite	$Ba_2Mn_8O_{16}$ or $Mn_{6.95}Fe_{0.64}Al_{0.26}Si_{0.02}Ba_{0.47}K_{0.33}Pb_{0.11}Na_{0.11}O_{16}H_{1.41}$	37.4	41.3	27.1	6
Cryptomelane	$(K_{1.3}Na_{0.22}Sr_{0.16})(Mn_{0.9475}Fe_{0.0375}Al_{0.025})_8O_{16}$	33.2	32	41.9	2.1
Braunite	$CaMn_{11.62}Fe_{2.38}SiO_{24}$	10.4	0	0	0
Calcite	$Ca(CO_3)$	8.4	0	0	0
Bixbyite	Mn_2O_3	6.4	18.9	31	2.2
Quartz	SiO_2	4.3	7.8	0	2.8
Hausmannite	Mn_3O_4	0	0	0	61.7
Amesite	$(Mg_2Al)(AlSiO_5)(OH)_4$	0	0	0	7.1
Calcium Magnesium Aluminum Oxide	$Ca_{0.965}Mg_2Al_{16}O_{27}$	0	0	0	16.6
Hematite	Fe_2O_3	0	0	0	1.4

* RT is the room temperature.

Table 7. Semi-quantitative phase ratios of braunite-psilomelane oxide manganese ore sample.

Mineral	**Chemical formula**	Fraction, %			
		at RT	Sintering temperature, °C		
			600	800	1000
Hollandite	$Ba_2Mn_8O_{16}$ or $Mn_{6.95}Fe_{0.64}Al_{0.26}Si_{0.02}Ba_{0.47}K_{0.33}Pb_{0.11}Na_{0.11}O_{16}H_{1.41}$	25.1	0	0	0
Bixbyite	Mn_2O_3	20.5	30.7	38.9	69.1
Quartz	SiO_2	45.5	69.3	54.6	30.9
Pyrolusite	MnO_2	8.9	0	0	0
Hausmannite	Mn_3O_4	0	0	6.5	0

* RT is the room temperature.

After sintering in each temperature range, it was found that the change of elemental concentration values does not change much. An increase in the uniformity of the structure indicates changes in the crystal lattices of the ore components resulting from phase transitions with a decrease in the number of phases. Figures 3 and 4 show the diagrams of the dependence of the phase composition of complex oxide manganese ore samples on the temperature regime, respectively.

Preprints.org (www.preprints.org) | NOT PEER-REVIEWED | Posted: 1 February 2024 doi:10.20944/preprints202402.0052.v1

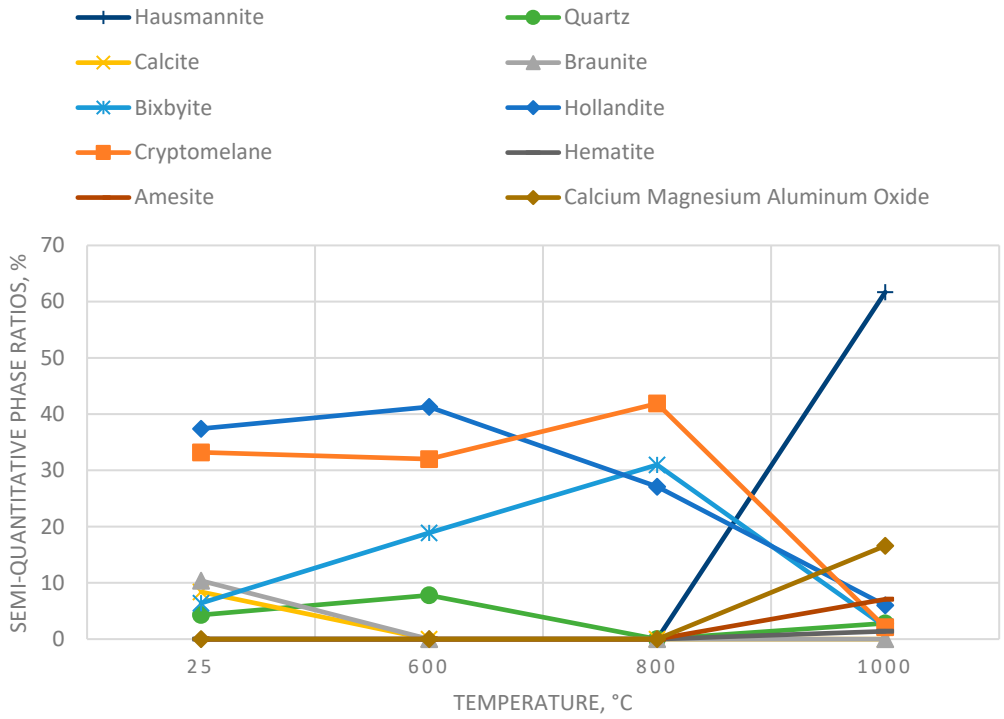

Figure 3. Dependence of the phase ratios of braunite-hematite manganese ore on the sintering temperature.

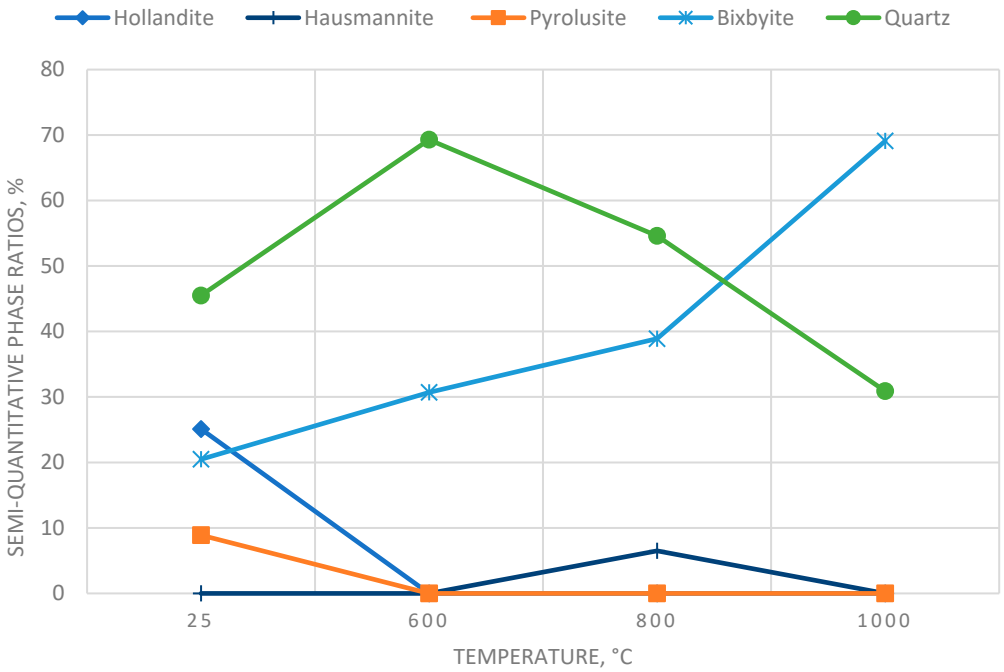

Figure 4. Dependence of the phase ratios of braunite-psilomelane oxide manganese ore on the sintering temperature.

The results obtained in this study are in good correlation with those obtained in some previous researches. In [12] hausmannite nanoparticles were synthesized from manganese ore of the West Sumatera deposit. The products were characterized using methods like X-Ray Fluorescence (XRF) for composition analysis, X-Ray Diffraction (XRD) for crystal structure and size, and Scanning Electron

 doi:10.20944/preprints202402.0052.v1

Microscopy (SEM) for surface morphology. The results showed that the sintering process affects the phase formation of hausmannite nanoparticles. The hausmannite phase occurs at a sintering temperature of 700°C. The sintering temperature variations help in obtaining the hausmannite phase from the manganese ore used in the study. The high-energy milling time affects particle size, with a reduction to nano size at 8 hours and subsequent agglomeration at 10 hours. The smallest average grain size obtained was 90.50 nm after 8 hours of milling. Similar results were found in [10] where manganese powders were synthesized using the dry precipitation method, with natural manganese ore phases as the initial material. The crystal structure and grain size of manganese were dependent on the sintering temperature. Changes in the sintering temperature resulted in alterations in the structure of the formed manganese oxide. Furthermore, the sintering temperature affected the size of the manganese oxide grains formed. In the case of the hausmanite phase, the grain size increased with an increase in the sintering temperature.

The analysis of the previously obtained results summarizes the vectors for the subsequent research experiments. The study results can include the nanomilling stage in the process, as well as widening the temperature range up to 1100°C.

4. Conclusions

In this research, braunite-hematite and braunite-psilomelane oxide manganese ores were studied. Elemental and phase contents of the ores were studied in the initial state (25 °C) and after sintering at temperatures 600, 800, and 1000 °C. Before sintering, the samples were milled for 8 hours in a ball mill. The size of obtained particles was less than 0.071 mm. Changes in elemental and phase composition after the sintering process were investigated using EDX and XRD methods. The research determined the dependencies of the phase and elemental composition of the studied ores on the sintering temperature. The following main results were obtained:

1. The original mineral base of the studied braunite-hematite ore was hollandite, cryptomelane, and braunite. Calcite, bixbyite, and quartz are presented as impurities. The initial mineral base of the braunite-psilomelane oxide ore consists of hollandite, bixbyite, and pyrolusite. This sample contains a significant amount of quartz (45.5 %). The average elemental content of Mn was 83.3% for braunite-hematite ore and 70.9% for braunite-psilomelane oxide ore. The EDX spectral analysis has shown the high homogeneity in the Mn elemental content of the braunite-hematite ore and, consequently, in the ore structure.

2. Based on the data obtained by the semi-quantitative X-ray phase analysis method, a change in the sintering temperature affects the formation of manganese oxide phases. With an increase in temperature, the phases change, passing from one mineral type to another, similar to geological metamorphic processes in the earth's crust. After temperature treatment, phase transformations of the samples led to the formation of more thermostable phases such as bixbyite and hausmannite.

3. For the braunite-hematite ore, hausmannite is the most stable phase at high temperatures. The bixbyite-hausmannite phase transition for this ore sample occurs at a temperature of 1000 °C, and hausmannite fraction reaches 61.7%. At the final stage, the presence of the original mineral phases is minimized except for calcium-magnesium spinels (calculated ratio was up to 16.6%).

4. The heterogeneous braunite-psilomelane oxide ore has a slightly different nature of the phase transitions. The hausmannite phase is formed at lower temperatures than in the previous ore sample. At a temperature of 800 °C, a transition of hausmannite with a phase ratio of 6.5% was observed. The phase transformations also involved pyrolusite MnO_2 (IV), which was present in a fraction of 8.9% in the initial state and was reduced to manganese (III) oxide during sintering. However, at 1000 °C, hausmannite was not detected, and bixbyite was obtained as the main phase.

5. EDX analysis has shown that the high-temperature phase modifications decreased elemental content variations and, consequently, increased the uniformity of structure. That increase in structure uniformity possibly appears because of the minimized number of thermal-stable phases. Thus, in both samples, the initial four major phases were transformed into two major stable phases after sintering.

Thus, the studied manganese ores are promising raw materials for various processes of technological processing. The studied braunite-hematite and braunite-psilomelane oxide ores open prospects for producing products based on thermally stable hausmannite and bixbyite phases. Finding optimal conditions for sintering can allow for obtaining the optimal phase content of the product.

Author Contributions: Conceptualization, R.Z.S., N.I.V. and J.B.K.; data curation, R.Z.S., J.B.K., A.K.Zh. and Ye.K.A., methodology, N.I.V., R.Z.S., J.B.K. and C.H.W.B.; validation, L.d.L.S.V. and J.S.; formal analysis, N.I.V. and Ye.K.A.; resources, A.K.Zh. and R.Z.S.; writing—original draft preparation, A.K.Zh., R.Z.S.; writing—review and editing, N.I.V. and L.d.L.S.V.; supervision, C.H.W.B.; project administration J.B.K.; Funding acquisition, R.Z.S.; Investigation, R.Z.S., A.K.Zh., Software's, R.Z.S. and A.K.Zh., Visualization, R.Z.S. and L.d.L.S.V. All authors have read and agreed to the published version of the manuscript.

Funding: The given research was carried out within the framework of a project funded by the Science Committee of the Ministry of Science and Higher Education of the Republic of Kazakhstan (Grant No.AP23488858). This research was funded by the Ministry of Science and Higher Education of the Russian Federation within the framework of the state assignment No. 075-03-2022-010 dated 14 January 2022 and No. 075--01568-23-04 dated 28 March 2023(Additional agreement 075-03-2022-010/10 dated 09 November 2022, Additional agreement 075-03-2023-004/4 dated 22 May 2023), FSEG-2022-0010.

Acknowledgments: The experimental works were partly performed at Cavendish Laboratory, Canbridge University (Cambridge, UK) during the scientific internship "500 scientists" by the Ministry of Science and Higher Education of the Republic of Kazakhstan. We would like to express our special gratitude to Galiya Bekenova (Institute of Geological sciences named after K.I. Satpaev, Almaty, Kazakhstan) for significant support in conducting the physical-chemical analyses, and all of the people supporting this research.

Conflicts of Interest: The authors declare no conflict of interest.

References

1. Pérez, K.; Toro, N.; Robles, P.; Gallegos, S.; Gálvez, E.; González, F.J.; Marino, E.; Hernández, P.C. Cobalt and Manganese Extraction from Ocean Nodules by Co-Processing with Steel Metallurgical Slag. *Metals* **2023**, *13*. https://doi.org/10.3390/met13061079.
2. Yu, D.; Cui, F.; Cong, Y.; Zhang, C.; Tian, Q.; Guo, X. Simultaneous Selective Chlorination and Carbothermic Reduction of High-Iron Manganese Ore for the Recovery of Manganese Chloride and Metallic Iron. *Metals* **2019**, *9*. https://doi.org/10.3390/met9101124.
3. Xiao, J.; Zou, K.; Chen, T.; Xiong, W.; Deng, B. Extraction of Manganese and Iron from a Refractory Coarse Manganese Concentrate. *Metals* **2021**, *11*. https://doi.org/10.3390/met11040563.
4. Liu, Y.; He, F.; Ma, D.; Hu, Q.; You, Z. Novel Process of Reduction Roasting Manganese Ore with Sulfur Waste and Extraction of Mn by Acid Leaching. *Metals* **2022**, *12*. https://doi.org/10.3390/met12030384.
5. Kies, F.; Wilms, M.B.; Pirch, N.; Pradeep, K.G.; Schleifenbaum, J.H.; Haase, C. Defect Formation and Prevention in Directed Energy Deposition of High-Manganese Steels and the Effect on Mechanical Properties. *Materials Science and Engineering A* **2020**, *772*. https://doi.org/10.1016/j.msea.2019.138688.
6. Sosnovskii, L.A.; Baglyuk, G.A.; Vlasova, O.V.; Golovkova, M.E. Structure and Properties of Sintered Silicon–Manganese Steels. *Powder Metallurgy and Metal Ceramics* **2015**, *53*, 657–662. https://doi.org/10.1007/s11106-015-9671-1.
7. Gamutan, J.; Miki, T.; Nagasaka, T. Morphology and Composition of Inclusions in Si-Mn Deoxidized Steel at the Solid-Liquid Equilibrium Temperature. *ISIJ International* **2020**, *60*, 84–91. https://doi.org/10.2355/isijinternational.ISIJINT-2019-313.
8. Ali, S.; Iqbal, Y.; Fahad, M. A Comprehensive Phase, Minero-Chemical and Microstructural Investigation of Low-Grade Manganese Ore. *Materials Research Express* **2019**, *6*, 115527–115527. https://doi.org/10.1088/2053-1591/ab4c23.
9. Vodyanitskii, Yu.N. Mineralogy and Geochemistry of Manganese: A Review of Publications. *Eurasian Soil Sc.* **2009**, *42*, 1170–1178. (en). https://doi.org/10.1134/S1064229309100123.
10. Fauzi, A.; Ratnawulan; Putri, P.J. Effect of Sintering Temperature on Crystal Structure and Grain Size of Manganese Ores from West Sumatera.; 2018; Vol. 1040. https://doi.org/10.1088/1742-6596/1040/1/012051.

11. Rani, B.J.; Ravina, M.; Ravi, G.; Ravichandran, S.; Ganesh, V.; Yuvakkumar, R. Synthesis and Characterization of Hausmannite (Mn3O4) Nanostructures. *Surfaces and Interfaces* **2018**, *11*, 28–36. https://doi.org/10.1016/j.surfin.2018.02.007.
12. Ratnawulan; Prasetyo, F.; Fauzi, A.; Ramli Synthesis and Characterization Hausmannite (Mn3O4) Nanoparticle of Manganese Ores Prepared By High-Energy Milling. *International Journal of Advanced Science and Technology* **2020**, *29*, 8332–8339, url:https://www.scopus.com/record/display.uri?eid=2-s2.0-85083833012&origin=inward&txGid=63f20a0a5afa387d2f116e1ab9529b2c.
13. Reddy, U.M.; Gopalkrishna, S.J.; Kumar, P.S.; Hatti, B. Characterization and Processing of Low Grade Iron Rich Manganese Ore. *International Journal of Scientific and Technology Research* **2019**, *8*, 2448–2451, url:https://www.scopus.com/inward/record.uri?eid=2-s2.0-85077337156&partnerID=40&md5=f6c3f28bd96e27dfbc96f139da3a1a7a.
14. Sukhdev, A.; Challa, M.; Narayani, L.; Manjunatha, A.S.; Deepthi, P.R.; Angadi, J.V.; Mohan Kumar, P.; Pasha, M. Synthesis, Phase Transformation, and Morphology of Hausmannite Mn3O4 Nanoparticles: Photocatalytic and Antibacterial Investigations. *Heliyon* **2020**, *6*, e03245. https://doi.org/10.1016/j.heliyon.2020.e03245.
15. Aripin, H.; Priatna, E.; Busaeri, N.; Hiron, N.; Sabchevski, S. Reduction Behavior of Medium Grade Manganese Ore from Karangnunggal during a Sintering Process in Methane Gas.; 2019; Vol. 550. https://doi.org/10.1088/1757-899X/550/1/012036.
16. Moradkhani, D.; Malekzadeh, M.; Ahmadi, E. Nanostructured MnO2 Synthesized via Methane Gas Reduction of Manganese Ore and Hydrothermal Precipitation Methods. *Transactions of Nonferrous Metals Society of China (English Edition)* **2013**, *23*, 134–139. https://doi.org/10.1016/S1003-6326(13)62439-5.
17. Sorensen, B.; Gaal, S.; Tangstad, M.; Ringdalen, E.; Kononov, R.; Ostrovski, O. Properties of Manganese Ores and Their Change in the Process of Calcination.; 2010; pp. 439–448.
18. Fujii, Y.; Nakai, Y.; Uchida, Y.-I.; Miki, Y. Fundamental Investigation of High Temperature Reduction and Melting Behavior of Manganese Ore. *ISIJ International* **2017**, *57*, 609–614. https://doi.org/10.2355/isijinternational.ISIJINT-2016-568.
19. Brustad, O.K.; Låstad, J.; Hoseinpur, A.; Safarian, J. Characterization, Calcination and Pre-Reduction of Polymetallic Manganese Nodules by Hydrogen and Methane. *Metals* **2022**, *12*. https://doi.org/10.3390/met12122013.
20. Li, P.; Luo, S.-H.; Wang, X.; Wang, L.; Wang, J.; Teng, F.; Wang, Q.; Zhang, Y.; Liu, X.; Zhang, H.; et al. Study on the High-Efficiency Separation of Fe and Mn from Low-Grade Pyrolusite and the Preparation of LiMn2O4 Materials for Lithium-Ion Batteries. *Separation and Purification Technology* **2022**, *278*. https://doi.org/10.1016/j.seppur.2021.119611.
21. Feng, W.; Faraj, Y.; Yan, Y.; An, Y.; Xie, R.; Lai, B. Novel Pyrolusite-Templated Biochar as an Outstanding Catalyst for Persulfate Activation: Structural Design, Synergistic Effect, and Mechanism. *Industrial and Engineering Chemistry Research* **2022**, *61*, 1885–1896. https://doi.org/10.1021/acs.iecr.1c04459.
22. Flook, R. Manganese: The Black Art. *Benchmark Mineral Intelligence* **2019**, *1*, 38–47, url:https://www.element25.com.au/site/PDF/1771_0/BenchmarkMineralIntelligenceManganeseTheBlackArt.
23. Deraz, N.M. Green Synthesis, Characterization and Magnetic Properties of Hausmannite Nanoparticles. *Acta Physica Polonica A* **2019**, *136*, 147–150. https://doi.org/10.12693/APhysPolA.136.147.
24. Pligin, E.I.; Lavysh, A.V.; Lugovskii, A.A.; Voropay, E.S.; Kopishev, É.E.; Maskevich, A.A. Luminescence Spectral Properties of New Benzothiazole Polymethine Dye. *Journal of Applied Spectroscopy* **2023**, *89*, 1021–1028. https://doi.org/10.1007/s10812-023-01461-6.
25. Chen, S.; Li, H.; Hao, Y.; Chen, R.; Chen, T. Porous Mn-Based Oxides for Complete Ethanol and Toluene Catalytic Oxidation: The Relationship between Structure and Performance. *Catal. Sci. Technol.* **2020**, *10*, 1941–1951. (en). https://doi.org/10.1039/C9CY02522G.
26. Pulleri, J.K.; Singh, S.K.; Yearwar, D.; Saravanan, G.; Al-Fatesh, A.S.; Labhasetwar, N.K. Morphology Dependent Catalytic Activity of Mn3O4 for Complete Oxidation of Toluene and Carbon Monoxide. *Catal Lett* **2021**, *151*, 172–183. (en). https://doi.org/10.1007/s10562-020-03278-w.
27. Akylbekov, S.A. Manganese of Kazakhstan. *News of the National Academy of Sciences of the Republic of Kazakhstan, Series of Geology and Technical Sciences* **2006**, 42–53. (Russian), url:http://nblib.library.kz/elib/library.kz/Jurnal/g_2006_1/42-53.pdf.

28. Zhuniskaliyev, T.; Nurumgaliyev, A.; Zayakin, O.; Mukhambetgaliyev, Y.; Kuatbay, Y.; Mukhambetkaliyev, A. Investigation and Comparison of the Softening Temperature of Manganese Ores Used for the Production of Complex Ligatures Based on Fe-Si-Mn-Al. *Metalurgija* **2020**, *59*, 521–524. (en), url:https://hrcak.srce.hr/en/241208.
29. Yushko, S.A.; Lazur, Y.M. Mineral Associations of the Zhaksy-Kotr Manganese Deposit (Central Kazakhstan). *International Geology Review* **1979**, *21*, 403–407. https://doi.org/10.1080/00206818209467072.
30. Berdenov, Zh.G.; Mendybayev, E.H.; Ataeva, G.M.; Dzhanaleeva, G.M. Landscape and Geochemical Features of Man-Made Pollution Zones of Aktobe Agglomerations. *Oxidation Communications* **2015**, *38*, 852–859.
31. Liu, J.; Baeyens, J.; Deng, Y.; Wang, X.; Zhang, H. High Temperature Mn2O3/Mn3O4 and Co3O4/CoO Systems for Thermo-Chemical Energy Storage. *Journal of Environmental Management* **2020**, *267*, 110582. (en). https://doi.org/10.1016/j.jenvman.2020.110582.
32. Alonso, E.; Hutter, C.; Romero, M.; Steinfeld, A.; Gonzalez-Aguilar, J. Kinetics of Mn2O3–Mn3O4 and Mn3O4–MnO Redox Reactions Performed under Concentrated Thermal Radiative Flux. *Energy Fuels* **2013**, *27*, 4884–4890. https://doi.org/10.1021/ef400892j.
33. Jacob, K.T.; Kumar, A.; Rajitha, G.; Waseda, Y. Thermodynamic Data for Mn3O4, Mn2O3 and MnO2. *High Temperature Materials and Processes* **2011**, *30*. https://doi.org/10.1515/htmp.2011.069.
34. Bielsa, D.; Zaki, A.; Faik, A.; Arias, P.L. Efficiency Improvement of Mn2O3/Mn3O4 Redox Reaction by Means of Different Operation Strategies.; 2019; Vol. 2126. https://doi.org/10.1063/1.5117750.
35. Dubal, D.P.; Dhawale, D.S.; Salunkhe, R.R.; Pawar, S.M.; Lokhande, C.D. A Novel Chemical Synthesis and Characterization of Mn 3 O 4 Thin Films for Supercapacitor Application. *Applied Surface Science* **2010**, *256*, 4411–4416. https://doi.org/10.1016/j.apsusc.2009.12.057.
36. Hewett, D.F.; Fleischer, M. Deposits of the Manganese Oxides. *Economic Geology* **1960**, *55*, 1–55. https://doi.org/10.2113/gsecongeo.55.1.1.
37. Jarosch, D. Crystal Structure Refinement and Reflectance Measurements of Hausmannite, Mn3O4. *Mineralogy and Petrology* **1987**, *37*, 15–23. https://doi.org/10.1007/BF01163155.
38. Baron, V. The Influence of Iron Substitution on the Magnetic Properties of Hausmannite, Mn2+(Fe,Mn)23+04. *American Mineralogist* **1998**, *83*, 786–793. https://doi.org/10.2138/am-1998-7-810.
39. Hausmannite Mineral Data Available online: http://www.webmineral.com/data/Hausmannite.shtml (accessed on 8 February 2023).
40. Durdubaeva, R.; Beknazarov, H.; Asamatdinov, A.; Yusupova, N. Study of Steel Corrosion Inhibition with the Use of Secondary Waste. *BULLETIN of the L.N. Gumilyov Eurasian National University. Chemistry. Geography. Ecology Series* **2022**, *138*, 31–36. https://doi.org/10.32523/2616-6771-2022-138-1-31-36.
41. Laffont, L.; Gibot, P. High Resolution Electron Energy Loss Spectroscopy of Manganese Oxides: Application to Mn3O4 Nanoparticles. *Materials Characterization* **2010**, *61*, 1268–1273. https://doi.org/10.1016/j.matchar.2010.09.001.
42. Fauzi, A.; Lidia, B.; Ratnawulan, R.; Ramli, R. Structural Analysis of the Hausmannite Thin Film (Mn3O4) by Spin Coating Method.; 2019; Vol. 1185. https://doi.org/10.1088/1742-6596/1185/1/012032.